

1 Improved Quality Metrics for Association and Reproducibility in
2 Chromatin Accessibility Data Using Mutual Information

3 Cullen Roth^{1,*}, Vrinda Venu², Vanessa Job³, Nicholas Lubbers⁴, Karissa Y. Sanbonmatsu⁵,
4 Christina R. Steadman², and Shawn R. Starkenburg¹

5 ¹Los Alamos National Laboratory, Genomics and Bioanalytics, Los Alamos, New Mexico

6 ²Los Alamos National Laboratory, Climate, Ecology and Environment, Los Alamos, New Mexico

7 ³Los Alamos National Laboratory, High Performance Computing and Design, Los Alamos, New Mexico

8 ⁴Los Alamos National Laboratory, Information Sciences, Los Alamos, New Mexico

9 ⁵Los Alamos National Laboratory, Theoretical Biology and Biophysics, Los Alamos, New Mexico

10 * Corresponding Author: croth@lanl.gov

11 June 2023

12 Abstract

13 Background

14 Correlation metrics are widely utilized in genomics analysis and often implemented with little regard to
15 assumptions of normality, homoscedasticity, and independence of values. This is especially true when com-
16 paring values between replicated sequencing experiments that probe chromatin accessibility, such as assays
17 for transposase-accessible chromatin via sequencing (ATAC-seq). Such data can possess several regions
18 across the human genome with little to no sequencing depth and are thus non-normal with a large portion
19 of zero values. Despite distributed use in the epigenomics field, few studies have evaluated and benchmarked
20 how correlation and association statistics behave across ATAC-seq experiments with known differences or
21 the effects of removing specific outliers from the data. Here, we developed a computational simulation of
22 ATAC-seq data to elucidate the behavior of correlation statistics and to compare their accuracy under set
23 conditions of reproducibility.

24 Results

25 Using these simulations, we monitored the behavior of several correlation statistics, including the Pearson's
26 R and Spearman's ρ coefficients as well as Kendall's τ and Top-Down correlation. We also test the behavior
27 of association measures, including the coefficient of determination R^2 , Kendall's W , and normalized mutual
28 information. Our experiments reveal an insensitivity of most statistics, including Spearman's ρ , Kendall's τ ,
29 and Kendall's W , to increasing differences between simulated ATAC-seq replicates. The removal of co-zeros
30 (regions lacking mapped sequenced reads) between simulated experiments greatly improves the estimates of
31 correlation and association. After removing co-zeros, the R^2 coefficient and normalized mutual information
32 display the best performance, having a closer one-to-one relationship with the known portion of shared,
33 enhanced loci between simulated replicates. When comparing values between experimental ATAC-seq data
34 using a random forest model, mutual information best predicts ATAC-seq replicate relationships.

35 Conclusions

36 Collectively, this study demonstrates how measures of correlation and association can behave in epigenomics
37 experiments. We provide improved strategies for quantifying relationships in these increasingly prevalent
38 and important chromatin accessibility assays.

39 Keywords

40 ATAC-seq; Correlation and Association; Normalized Mutual Information; Random Forest

41 Background

42 Epigenetic modifications play an important role in regulating multiple cellular processes ranging from DNA
43 replication to gene expression. These covalent additions to DNA and histone proteins do not alter the
44 underlying DNA sequence, but rather, help modulate chromatin structure resulting in distinctive phenotypes.
45 Genome-wide epigenetic modifications can be determined using several techniques: the gold-standard is
46 chromatin immunoprecipitation followed by sequencing (ChIP-seq) [1, 2, 3]. Chromatin accessibility, or the
47 analysis of the regions that are available for DNA:protein interactions potentially resulting in gene expression,
48 is measured using an enzyme-driven assay called transposase-accessible chromatin via sequencing (ATAC-
49 seq) [4]. These two methods have distinct advantages in probing the state of the epigenome, and both
50 approaches generate paired-end sequencing libraries. These data are mapped to the genome to determine
51 the loci that are occupied with a particular epigenetic modification or the loci that are localized within an
52 open, accessible region. Epigenetic modifications and chromatin accessibility are visualized as peaks resulting
53 from the aggregation of sequencing reads [5]. As such, many software platforms used for analysis of ChIP-seq
54 and ATAC-seq data sets use ‘peak calling’ to determine locations of epigenetic modifications or accessible
55 chromatin regions [6, 7, 8, 9].

56 To ensure significance and consistency of identified peaks, best practices have been defined for quantifying
57 reproducibility across experimental replicates [8, 10]. These include several quality control metrics and work-
58 flows that standardize analysis and enable comparison among different experiments [10]. These standards
59 apply to the total number of sequenced reads, total number of identified significant peaks, and concentration
60 of sequenced reads within said peaks. For example, pseudo-replication was developed for ChIP-seq analysis
61 to assess the amount of variation between biological replicates [8]. In this protocol, synthetic replicates are
62 created from true, experimentally derived data: to do this, aligned reads are merged from two true replicates
63 and randomly reassigned into new alignments to create two synthetic replicates. This permutation practice
64 homogenizes (and splits) signals present within the true, observed replicates, generating the null hypothesis of
65 near perfect correlation between pseudo-replicates. Peak calling is then also conducted on pseudo-replicates,
66 and the read counts of peaks conserved between the two pseudo-replicates are compared to the observed
67 peaks in the true replicates. Landt *et al.* (2012) proposed that experiments, whose number of observed peak
68 counts (among true replicates) divided by the total number of pseudo peaks (between pseudo-replicates),
69 which nears a value of one, are broadly reproducible [8]. The ENCODE project has since extended this
70 practice to ATAC-seq experiments [11, 12].

71 To better understand experimental reproducibility, many studies also conduct correlation analysis on
72 binned signals between ATAC-seq replicates [13, 14, 15]. In such analyses, for each replicate, the genome is

73 binned into smaller, contiguous regions, for example using windows of ten kilobase pairs [13]. The number
74 of mapped sequenced fragments (defined by a pair of mapped reads) that overlap these bins are counted
75 and standardized to fragments per kilobase pair per million reads (Fpkm) [16]. These Fpkm counts are
76 then compared between replicates using correlation and association statistics such as Pearson's R or the
77 coefficient of determination (R^2), respectively. Values from these statistics trending toward a value of one
78 generally indicate a reproducible experiment [17].

79 Correlation analysis is a useful tool, not singularly purposed for the analysis of reproducibility in ATAC-
80 seq experiments. Such analysis can be found within studies of chromosome accessibility in cancer, ageing
81 of human stem cells, cellular diversity, or new ATAC-seq protocols [18, 19, 20, 21, 22, 23]. Furthermore,
82 correlation analyses are ubiquitous, found in the fields of genetics, RNA-seq experiments, and in studies of
83 3D chromatin architecture [24, 25, 26, 27, 28, 29, 30, 16]. Given their popularity and use in genomic and
84 epigenetic studies, software suites—for example deeptools and HiCExplorer—have developed methods and
85 tools for calculating correlation metrics between replicates and experiments [13, 31, 32, 33, 34].

86 The natural properties of data from genomic and epigenomic experiments make the application of com-
87 monly used correlation and association statistics, for example Pearson's R and R^2 , potentially problematic as
88 none of these data (ATAC-, ChIP-, or Hi-C seq) are normally distributed [35]. Both ATAC- and ChIP-seq ex-
89 periments are defined by numerous, loci-specific peaks of signal generated by the accumulation of sequencing
90 reads [3, 4]. Mapped sequenced fragments may overlap contiguous genomic bins used in analysis, producing
91 non-independent data points [24]. Conversely, regions lacking assayed modifications or with inaccessible
92 chromatin will have little to zero signal for ChIP-seq or ATAC-seq data, respectively. Furthermore, during
93 correlation analysis, several genomic bins may overlap an inaccessible chromatin region that is reproducible,
94 appearing in both the ATAC-seq replicates (or experiments) being compared. As such, each of these bins will
95 acquire zero Fpkm and within the bi-variate distribution formed between the replicates. These data points,
96 which appear as zero Fpkm in both replicates, are referred to here as co-zeros. Some analysis programs,
97 like deeptools, HiCExplorer, and HiCcompare, offer options to remove co-zeros prior to analysis [31, 34, 29].
98 However, there is no published guidance on this practice, and while the co-zero values are a feature common
99 across genomic and epigenomic data sets [36], the effect of removing such features on correlation statistics
100 has not been explored. Despite the known features of genomic and epigenomic data, and the underlying
101 assumptions of statistical tests, there have been few studies that explore their expected behavior, accuracy,
102 and use of alternative statistics determining reproducibility of such data [26, 27].

103 Here, we present a computational approach to generate synthetic ATAC-seq replicates to explore the
104 behavior of various correlation and association metrics for epigenomics datasets. These synthetic ATAC-seq
105 replicates are generated from eight true data sets to capture features uniquely present within ATAC-seq

106 experiments. We have developed a random subsampling strategy to generate synthetic replicates with
107 varying portions of shared peaks, as a proxy for reproducibility. Across our simulations, we apply the
108 Pearson's R [37, 38, 39] and Spearman's ρ [40] and monitor their behavior, including the effect of removing
109 co-zeros. Additionally, we demonstrate the behavior of other statistics, including non-parametrics such as
110 Kendall's τ [41, 42, 43, 44] and an information theoretic approach, normalized mutual information [45, 46], to
111 determine their utility in assessing epigenomics data. Finally, we build a random forest model [47] using the
112 normalized mutual information and R^2 coefficient between experiments to predict the biological relationships
113 between replicates. Overall, our results demonstrate an improvement in the expected behavior of all statistics
114 after removing co-zeros and normalized mutual information emerges as a promising statistic for measuring
115 association between ATAC-seq samples.

116 **Results**

117 **ATAC-seq data characteristics and subsampling strategy for synthetic replicate** 118 **generation**

119 To study the behavior of correlation measurements between ATAC-seq replicates, we analyzed data from
120 three experiments using the A549, human lung cell line and implemented a subsampling paradigm to generate
121 synthetic replicates. Across these experiments, the total number of reads mapped to the human reference
122 genome varied from 15 million to nearly 43 million (Table 1). The number of genome-wide peaks found in
123 the ATAC-seq samples varied across experiments and between replicates, ranging from approximately 80 to
124 130 thousand (Table 1). The fraction of sequenced read-pairs mapped in peaks (i.e. the Frip score as defined
125 by the ENCODE project [8, 11]), was greater than 0.34 for all of the A549 ATAC-seq samples (Table 1).
126 These samples displayed high spatial correlation of peaks across replicates (Figure 1A). Counting all whole
127 fragments per kilobase per million (WFpkm), every ten kilobases, we observed a high statistical correlation
128 between replicates, with average Pearson's R of 0.86, 0.87, and 0.94 (p -values < 0.05) between the technical
129 replicates of the three biological replicate experiments (Figure 1B).

130 For simulations, synthetic replicates were generated using the paired-end read alignment profiles from
131 the eight ATAC-seq samples we generated. For each simulation, two synthetic replicates were initiated by
132 duplicating a given true ATAC-seq experiment (Figure 2A). Within the true ATAC-seq data set, reproducible,
133 significant peaks were identified (see Methods). From these, a random portion of peaks was chosen to vary
134 between the two synthetic replicates. This was accomplished by subsampling 85% of the aligned sequenced
135 fragments within each of the randomly chosen peaks between the two synthetic replicates (Figure 2B and
136 2C). This process was repeated, randomly varying the common peaks from 1 to 95% of peaks between the
137 two synthetic replicates. Finally, across all simulations, for each pair of synthetic replicates, the WFpkm
138 values were calculated in ten kilobase windows and used in statistical comparisons (Figure 3A).

139 **Top-down correlation displays best behavior in correlation analysis across simu- 140 lations**

141 Across these down sampling simulations, correlation and association statistics were calculated between each
142 pair of synthetic replicates. The Wfpkm counts were used between synthetic replicates in statistical analysis
143 (Figure 3A). The values of correlation and association statistics were calculated across simulations, as a
144 function of the number of shared peaks between synthetic replicates (Figure 3B) and for each statistic, and
145 the area under the curve (AUC) was used in comparisons (Supplementary Figure S1). Of the correlation

146 statistics, the Top-Down correlation statistic had the smallest average AUC of 0.6881 (95% CI: 0.6860 –
147 0.6906) and was significantly smaller than the average AUC of the Pearson’s R , at 0.8284 (95% CI: 0.8237
148 – 0.8335, p -value = 0, bootstrapped difference of mean AUC). Both the two non-parametric statistics,
149 Spearman’s ρ and Kendall τ , had significantly larger average AUCs compared against the Pearson’s R
150 (p -values = 0, bootstrapped difference of mean AUC). However, they demonstrated nearly identical AUC
151 profiles compared to each other, with average AUC of 0.9140 (95% CI: 0.9118 – 0.9162) and 0.9096 (95%
152 CI: 0.9074 – 0.9120) respectively (p -value = 0.037, bootstrapped difference of mean AUC).

153 Across the metrics of association, Kendall’s W , normalized mutual information, and the R^2 coefficient,
154 between replicates, the R^2 coefficient exhibited the greatest sensitivity to the change in portion of shared
155 peaks between synthetic replicates (Figure 3B). Across simulations, the average AUC of the R^2 coefficient
156 was 0.7026 (95% CI: 0.6951 – 0.7102). This average AUC was significantly smaller than the average AUC
157 of the Kendall’s W and normalized mutual information, with values of 0.957 (95% CI: 0.9559 – 0.9581) and
158 0.8197 (95% CI: 0.8153 – 0.8241), respectively (p -value = 0, bootstrapped difference of mean AUC).

159 Removal of co-zeros improves estimates of correlation and associations

160 Using this simulation paradigm, we evaluated the efficacy of removing co-zeros from the analysis to determine
161 the impact on correlation and association statistics. Co-zero values were defined as value counts in ATAC-seq
162 experiments that appeared to have zero aligned fragments in a genomic bin of ten kilobases between two
163 replicates (Figure 3B, Supplementary Figure S2). On average, these values can make up nearly 5% of a
164 given bi-variate distribution formed between real ATAC-seq replicates (Supplementary Figure S3). Across
165 all the correlation and association statistics examined here—except for Top-Down correlation—removing the
166 co-zero values significantly reduced the average AUC (Table 2, Figure 3B, Supplementary Figure S1). This
167 finding was unexpected, as co-zeros are a modest portion of the bi-variate distribution formed between two
168 replicates and reproducible data points within the replicates.

169 After removing co-zeros, all the correlation statistics, Top-Down correlation, Pearson’s R , Spearman’s
170 ρ , and Kendall’s τ , displayed nearly identical sensitivity to the change in shared peaks between replicates
171 across simulations (Figure 3B). However, the Pearson’s R had the largest average AUC of 0.6965 (95% CI:
172 0.6946 – 0.6984) followed by the Top-Down statistic (AUC of 0.6872, 95% CI: 0.685 – 0.6895, p -value = 0,
173 bootstrapped difference of mean AUC). The Spearman’s ρ (mean AUC: 0.6686, 95% CI: 0.6665 – 0.6705) and
174 Kendall’s τ (mean AUC: 0.6673, 95% CI: 0.6654 – 0.6691) statistics had the smallest and identical average
175 AUC after removing co-zeros (p -value = 0.208, bootstrapped difference of mean AUC). Furthermore, the
176 AUC of the Top-Down correlation statistic was unaltered by the exclusion of co-zero values between synthetic

177 replicates (Figure 3B, Supplementary Figure S1, Table 2, p -value = 0.635, bootstrapped difference of mean
178 AUC). This observation was not surprising given how Top-Down correlation places emphasis on larger values,
179 down-weighting smaller values, such as co-zeros [48].

180 Normalized mutual information best estimates difference between replicates

181 Removing co-zero values had a similar effect on association metrics, attenuating and improving the average
182 AUC across the portion of shared peaks between synthetic replicates (Figure 3B, Supplementary Figure S1).
183 Apart from Kendall's W, the R^2 coefficient and normalized mutual information, on average, displayed a nearly
184 one-to-one relationship with the portion of shared peaks between replicates (Figure 3B). The average AUC of
185 normalized mutual information was 0.5055 (95% CI: 0.5045 – 0.5065) and was smaller than the average AUC
186 of the R^2 coefficient, with a value of 0.5346 (95% CI: 0.5324 – 0.5368, p -value = 0, bootstrapped difference
187 of mean AUC). This difference in average AUC indicates that normalized mutual information better follows
188 the designed proportion of shared peaks between synthetic replicates across our simulations, compared to
189 the R^2 coefficient.

190 As introduced earlier, one parameter in this simulation is the removal of a percentage of aligned read-pairs
191 from within randomly selected peaks (Figure 2B). Initially set at 85%, this parameter was altered to simulate
192 ATAC-seq replicates that are nearly reproducible (at 50%) at every selected peak or broadly unreproducible
193 (at 95%) across all selected peaks. Comparing the results between the two simulation sets with 85 and 95%
194 of reads removed, we observed no significant difference between the two simulations (see Supplementary
195 Data). This is somewhat expected when considering the small difference in magnitude between removing
196 85 and 95% of reads from within peaks. In simulations with only 50% of read pairs removed from selected
197 peaks, after removing co-zeros, the two statistics that showed the largest response in our simulation were
198 the R^2 coefficient and normalized mutual information (see Additional File 1 and Additional File 2).

199 Validation of mutual information analysis on true ATAC-seq data

200 After its successful implementation on simulated replicates, we next examined how normalized mutual in-
201 formation behaves when used on replicates from true ATAC-seq experiments. For this analysis, additional
202 ATAC-seq experiments were downloaded from the ENCODE project public repository [11]. These included
203 additional replicates of the A549 cell line, as well as ATAC-seq experiments in the HepG2, RWPE2, GM12878,
204 IMR-90, K562, and WTC11 cell lines (Table 1). With this expanded dataset, the Pearson's R , the Spear-
205 man's ρ , R^2 coefficient, and normalized mutual information were calculated between all pairs of replicates,
206 with co-zeros removed from analysis (Figure 4). Removing co-zeros reduced the estimates of correlation and

207 association across samples by approximately 0.18, 0.32, 0.23, and 0.30 on average for the Pearson's R , the
208 Spearman's ρ , R^2 coefficient, and normalized mutual information, respectively (Supplementary Figure S4A).
209 These differences were significantly greater than zero (p -value $< 10^{-10}$, Wilcoxon signed-rank test, Sup-
210 plementary Figure S4B). Between comparisons of true experiments, we observed a co-linear relationship in
211 the values of the normalized mutual information scores and R^2 coefficients (Figure 5A, Pearson's $R = 0.96$,
212 p -value $< 1^{-10}$). Of the four statistics, the R^2 coefficient displayed the largest variation ($\sigma^2 = 0.0329$)
213 between true replicates (Table 2).

214 Predicting replicate relationships using normalized mutual information

215 Given the comparable behavior between normalized mutual information and the R^2 coefficient on true ATAC-
216 seq replicates, we assessed their usefulness in predicting the relationships between experiments. To do this,
217 we utilized a random forest model, using the values of the R^2 coefficient and normalized mutual information
218 between true ATAC-seq experiments as features. Comparisons between any two ATAC-seq experiments
219 (either those from the ENCODE project or generated here) were classified into one of three discrete classes:
220 (1) between independent ATAC-seq experiments in different cell lines, (2) independent experiments using
221 the same cell line, and (3) between true replicates. Plotting the normalized mutual information against the
222 R^2 coefficient calculated between ATAC-seq experiments with the above classifications revealed clustering
223 of experimental relationships between replicates (Figure 5A).

224 To build our random forest model, we utilized ten-fold cross validation, stratifying on the replicate class.
225 An example confusion matrix from one of these folds demonstrates the model had difficulty distinguishing
226 between independent experiments using the same cell line and true, experimental replicates (Figure 5B).
227 This difficulty also manifested as lower f1-scores and recall for this class (Supplementary Figure S5). The
228 accuracy across these folds ranged from 88 to 98% (Figure 5C). Across the folds, the feature importance
229 score of the R^2 coefficient was inverted with that of normalized mutual information (Figure 5C). Overall, we
230 observed a greater feature importance score for normalized mutual information, with a significant average
231 pair-wise difference between the R^2 coefficient and normalized mutual information of 6.78% (p -value < 0.05 ,
232 Wilcoxon signed-rank test).

233 Discussion

234 To improve the assessment of reproducibility in epigenomic data sets, we sought to investigate the use of
235 several correlation and association statistics on binned genomic signals. Our findings suggest that best
236 practices should include analyzing association between compared replicates (or experiments) via normalized
237 mutual information with binned, Fpkm counts rounded to the nearest whole integer, after the removal of
238 co-zero values as input. In choosing a correlation statistic, after removing co-zero values, our results indicate
239 little difference in the outputs from the Pearson's R , Spearman's ρ , Kendall's τ , or Top-Down correlation
240 statistics. Notably, from simulations, we observed that the Top-Down correlation statistic was unaffected
241 by the removal of co-zeros values. As such, this statistic should serve as an alternative for investigators if
242 binned co-zeros values between replicates are retained.

243 As part of this study, we generated highly correlated, new ATAC-seq experimental replicates of the A549
244 cell line. Our data highly correlates with previously published ATAC-seq data of the A549 cell line generated
245 by the ENCODE project. Using these data, we generated a novel simulation that utilizes down sampling
246 to generate replicates with known varying signals. While similar simulation studies have been conducted on
247 Hi-C sequencing data [30], to our knowledge, no prior study has examined the behavior of statistical metrics
248 on ATAC-seq data. That said, there are several statistics and methodologies that may be used to analyze
249 this data type, such as Poisson regression [49]. Improving on this simulation design could help generate a
250 framework that allows researchers to develop new statistical tools for hypothesis testing.

251 In our simulations, we observed that most statistics overestimate the correlation of signal between replicates.
252 One specific strategy we investigated to reduce this inflation was the removal of co-zeros, which is an
253 option present in several bioinformatic software suites [31, 34, 29]. Our analysis demonstrated that removal
254 of these values can provide a more accurate estimate of correlation between replicates as measured by the
255 known number of peaks between replicates. Interestingly, we never observed a correlation value that perfectly
256 trends with the designed number of peaks between synthetic replicates. We also did not observe negative
257 correlation values between the replicate Fpkm counts. The first of these observations can be explained by
258 background autocorrelation still present within our synthetic replicates. The second of these observations
259 may point to a limitation in the design of our simulation, as negative correlation values have been observed
260 in true ATAC-seq profiles [31, 20]

261 In epigenomics and chromatin accessibility data sets, biological interpretation of the data is dependent
262 upon visualization of "peaks" where accumulation of sequenced reads denotes the presence of a modification
263 or an accessible region. Regions with zero (or nearly zero) aligned sequenced reads are deemed unmodified
264 or inaccessible and largely ignored when interpreting data. Correlation statistics should provide biologists

265 with the confidence that replicates are truly comparable. As stated above, the inclusion of co-zeros seems to
266 inflate values of most correlation and association statistics. Thus, removal of co-zeros formed by the genomic
267 bins that overlap and account for inaccessible regions may be warranted.

268 Using our simulation, we also examined the behavior of three association statistics, which we distinguish
269 from the set of correlation statistics as those metrics ranging in value from zero to one. These association
270 statistics were the R^2 coefficient, normalized mutual information statistic, and Kendall's W. Prior to the
271 removal of co-zeros, the only association statistic that displayed any sensitivity to the change in shared peaks
272 between replicates was the R^2 coefficient. Co-zeros inflate the value of this statistic by reducing the total
273 summed error between data points during calculation. Similarly, co-zeros increase the information gained
274 between replicates when calculating the normalized mutual information score. In other words, knowing
275 a replicate has a value of zero at a given genomic bin provides information that there is a zero at the
276 corresponding bin within the other replicate. After removing co-zeros, we saw a large improvement in the
277 sensitivity of both these statistics.

278 Curiously, Kendall's W displayed the least sensitivity to the designed peak counts between synthetic
279 replicates. This statistic was of interest given Kendall's W is capable of simultaneously examining the ranks
280 of more than two input samples [50, 41]. This would have provided researchers with a statistical tool capable
281 of examining correlation among a full set (triplicate) of replicates within a single test, rather than multiple
282 pair-wise comparisons. Removing co-zeros did little to improve the sensitivity of this statistic. The other
283 statistic from Kendall, Kendall's τ , displayed similar performance to the other non-parametric statistic,
284 Spearman's ρ . This finding is contrary to other studies of Kendall's τ conducted in the fields of signal
285 processing and psychology [43, 44]. For analysis of genomic data, the Spearman's ρ is standard in deeptools'
286 correlation functions [13]

287 Of the statistics examined here, the R^2 coefficient and normalized mutual information score were the
288 most sensitive to the change in shared peaks between replicates (when co-zeros were removed). Comparison
289 of these two statistics revealed that normalized mutual information was the better-behaved statistic. This
290 behavior manifested as smaller AUC within simulations, less variation in values across simulations, and
291 smoother values between unrelated synthetic replicates. Similarly, the computational evidence provided by
292 our random forest model suggests that normalized mutual information was better at estimating experimental
293 relationships between true ATAC-seq replicates. Taken together, these results indicate that of the two met-
294 rics, normalized mutual information may be the stronger association metric for ATAC-seq data. Information
295 theoretic approaches, such as normalized mutual information, have been utilized in several other biological
296 fields, ranging from cancer genomics to fungal genetics [51, 52, 53, 54, 55, 56, 57]. Regarding ATAC-seq
297 data, a handful of other studies have specifically used mutual information in data integration, analysis, and

298 deep-learning of single-cell ATAC-seq profiles [58, 59]. For those investigator interested in using information
299 theoretic approaches, several of these functions are made easily available within the python, scikit learn
300 library [46].

301 Sparsity and zero mapped sequenced reads are not unique properties of ATAC-seq data. These extend
302 to genomic, Hi-C, ChIP-seq, and RNA-seq data sets. Imputation along with modified zero-inflated models
303 have been used with success for studying RNA sequencing data sets and detecting regions with differential
304 expression [60]. Simulations and models of sampling zero-genomic count data have been developed to under-
305 stand the effects of these values, particularly in the context of differential analysis [36]. Previous simulation
306 studies of ATAC-seq have been focused on generating ATAC-seq data, for pipeline development, or single-cell
307 ATAC-seq samples, to examined different approaches in their analysis [61, 62]. To our knowledge, this is
308 the first example of using a simulation approach for studying reproducibility and association of ATAC-seq
309 samples. Adapting strategies from these previous studies will help improve our simulation and expand it to
310 other genomic and epigenomic sequencing data. The current results of our study strongly suggest that nor-
311 malized mutual information is an appropriate metric for measuring reproducibility in chromatin accessibility
312 assays.

313 Conclusions

314 For this study, we produced eight ATAC-seq experiments using the A549 Cancer cell line. Across replicates,
315 these ATAC-seq samples are well correlated and reproducible. For investigations of chromatin accessibility
316 (particularly in the A549 cell line), these experiments are an additional resource for developing analysis
317 pipelines, peak detection algorithms, and machine learning approaches.

318 Leveraging the A549 ATAC-seq experiments, we designed a computational simulation to generate simu-
319 lated replicates. Specifically, synthetic replicates were coded that share a known, fixed portion of significantly
320 enriched loci. Using these replicates, correlation metrics—the Pearson’s R , Spearman’s ρ , Top-Down, and
321 Kendall’s τ —and association statistics (ranging from zero to one—the R^2 coefficient, Kendall’s W , and nor-
322 malized mutual information—were tested for accuracy. Overall, the reported value of these statistics was
323 inflated and much larger than the fixed portion of shared, significant loci between replicates.

324 Removing specific outliers from ATAC-seq data, specifically the removal of co-zeros, improved estimates
325 of correlation and association. We estimate that co-zero values, when comparing WFpkm counts between two
326 real ATAC-seq experiments, occupy nearly five percent of a bi-variate distribution. While only a small portion
327 of the total data, filtering these values from analysis greatly improves the measurements of most correlation
328 and association statistics between samples, in simulation. Applied to real ATAC-seq data, removing co-zero
329 values from comparison significantly reduced the reported correlation and association statistic, matching
330 results from simulation.

331 One of the association statistics examined here is normalized mutual information, an information theoretic
332 approach that is less well known across the (epi)genomics field. After removing co-zero values, normalized
333 mutual information displayed the lowest inflation relative to the similarity between simulated replicates.
334 The R^2 coefficient also performed well in simulations (after removal of co-zeros), displaying good sensitiv-
335 ity to differences between simulated replicates. Of these two association metrics, a random forest model
336 selected normalized mutual information as the stronger feature when estimating experimental relationships
337 between real ATAC-seq experiments. From these results we conclude that normalized mutual information is
338 a powerful, non-parametric approach for estimating association between ATAC-seq experiments.

339 Methods

340 Construction of A549 ATAC-seq libraries

341 ATAC-seq experimental libraries were generated using A549 human lung carcinoma epithelial cells (ATCC,
342 VA, catalog #CCL-185) [63, 64, 65]. Three biological replicate libraries were prepared from freshly harvested
343 cells using an ATAC-seq kit (Active Motif, 53150) following the manufacturer's protocol. The remaining
344 five libraries were prepared using cryopreserved cells following methods outlined in Milani *et al.* (2016) with
345 modifications [18]. Briefly, A549 cells were cultured in T75 flasks and harvested by trypsinization using
346 0.25% (w/v) Trypsin-EDTA (0.5%) solution (Gibco, 15400054). Harvested cells were centrifuged and pellets
347 resuspended in freezing media containing DMEM (Gibco, 11885-084), 10% FBS (Corning, 35-015-CV), and
348 10% DMSO (ATCC, 4-X). Pellets were frozen using an isopropyl alcohol chamber (Thermo Fisher Scientific,
349 5100-0001) at -80°C. After 24 hours, frozen cells were transferred to liquid nitrogen for long term storage.
350 To perform experiments, cryopreserved cells were transferred to -80°C for several days, and the tube was
351 immersed in 37°C water bath for approximately two minutes on the day libraries were prepared. Thawed cells
352 were resuspended in 1X PBS with protease inhibitor cocktail (Thermo Fisher Scientific, 78430). Cell counts
353 and viability were assessed and aliquots containing 80,000 cells per sample were processed into ATAC-seq
354 libraries.

355 Sequencing, alignment and filtering

356 ATAC-seq libraries were sequenced at the sequencing facility at Los Alamos National Laboratory on an
357 Illumina NextSeq2000 sequencer in paired end mode (PE151) using P3 chemistry. With Fastp, raw reads
358 were trimmed and filtered to remove Nextra adaptors and reads with repetitive sequences [66]. Additionally
359 reads were also filtered to remove bases with low quality scores ($q < 15$). These processed reads were aligned
360 to the new, telomere-to-telomere human reference genome, version 2 [67] via bwa [68]. After alignment,
361 duplicate sequenced pairs were marked via samblaster and removed from analysis [69]. Read pairs mapping
362 to the mitochondria were also removed (see Supplementary Table S1).

363 Other data used

364 Raw ATAC-seq data, in the form of paired fastq.gz files, was downloaded from the ENCODE project for
365 the A549, HepG2, RWPE2, GM12878, IMR-90, K562, and WTC11 cell lines [70, 11]. The ENCODE file
366 experiment and replicate accession numbers are included in Table 1. For alignment, these data were passed
367 through the same pipeline described above for ATAC-seq samples generated here, and aligned to the human,

368 telomere-to-telomere, reference genome [67].

369 Peak calling, peak filtering and reproducibility

370 After filtering, sample alignments were analyzed to identify loci displaying significant enrichment of paired-end reads. This peak calling was conducted using MACS2 [6, 71]. Specifically, after removing duplicates and mitochondrial mapped reads, samples were further filtered using samtools with the following flags:
373 `-F 4 -F 256 -F 512 -F 1024 -F 2048 -q 30` and then passed to MACS2 in BAMPE mode [72, 73].

374 Between true, biological replicates, reproducible peaks were identified via irreproducible discovery rate thresholding [74]. Using ChIP-R, replicate narrow peak files were filtered to retain only those peaks that
375 were consistent across all replicates; in ChIP-R, where command line parameter, m = number of biological
376 replicates [75]. In addition to this setting the '`-fragment`' option was also invoked. These sets of final peak
377 counts were retained for further analysis.

379 Genomic down-sampling and simulation design

380 For each of the eight ATAC-seq experiments of A549 cells generated in this study, synthetic replicates were
381 generated by duplicating a given sample into two copies and then randomly, varying the total number of
382 shared peaks between them. Specifically, for a given ATAC-seq experiment, a set portion of peaks was
383 chosen at random, such that within one of the synthetic replicates, a given selected peak was depleted,
384 randomly removing a portion of the alignments within the peak bounds (as defined by MACS2). These
385 sets of peaks were randomly selected from the set of reproducible peaks for that sample and its associated
386 biological replicates (see above). Three sets of simulations were conducted, removing 50, 85 and 95% of reads
387 within selected peaks. This procedure results in two synthetic ATAC-seq replicates, generated from a single,
388 true parent ATAC-seq data set. These synthetic 'sister' ATAC-seq data sets have identical genome-wide
389 alignments except within a sub-set of loci that vary between them. From each true ATAC-seq data set,
390 synthetic sister replicates were generated by varying the total percentage of shared peaks from 99 to 5%,
391 with a delta of 5%. For each simulation, across the change in portion of shared peaks, a common random
392 seed was used to preserve autocorrelation across this axis. This process was repeated fifteen times for each
393 of the eight, A549 ATAC-seq samples, totaling a one hundred and twenty simulations.

394 Genomic binning, fragment counts, and standardization

395 On both synthetic samples from simulation studies or replicates from (true) ATAC-seq experiments, a genomic
396 binning approach was used to estimate correlation and association statistics between samples. For

397 each chromosome, contiguous bins were established 5'-3', every ten kilobases. Within each of these bins, the
398 number of sequenced fragments is counted and standardized to fragments per kilobase per million. These
399 counts were rounded up to their nearest whole integer generating standardized counts of whole fragments
400 per kilobase per million (WFpkm).

401 **Calculating correlation and association metrics**

402 In python scripts, using the `scipy-stats` module [76], the Pearson's R , Spearman's ρ , and Kendall's τ were
403 calculated on the WFpkm counts between pairs of ATAC-seq replicates. Functions for the Top-Down cor-
404 relation metric [48] and Kendall's W rank statistic [50, 41] were also developed using custom python code.
405 The R^2 coefficient was calculated using the square of the Pearson's R . The normalized mutual information
406 statistic from pythons `sklearn` module [46] was used in association studies. Between any pair of WFpkm
407 counts, the bi-variate distribution was examined to identify instances were both profiles contained a value
408 of zero WFpkm. For studies of the effects of co-zero inflation, these co-zero values were removed, and the
409 correlation (or association) statistics recalculated on these filtered distributions.

410 For correlation analysis on ATAC-seq experiments conducted here using A549 cells, the Pearson's R
411 correlation statistic was calculated on WFpkm values between replicates with co-zeros removed. Similarly,
412 co-zeros were removed prior to calculating correlation and association statistics between replicates of ATAC-
413 seq data downloaded from the ENCODE project public repository.

414 **Statistical tests on area under the curve**

415 Across simulations, values of correlation and associations statistics were calculated as a function of the
416 designed portion of peaks between synthetic replicates. For each statistic tested, the 95% confidence interval
417 of the average area under the curve was calculated via bootstrapping, with a thousand iterations. This
418 was done for statistical profiles from simulations with and without co-zero values. For comparisons of the
419 average area under the curve, either between statistics or within the same statistic after removing co-zeros,
420 one thousand permutations were used to calculate the null distribution of the difference between the mean
421 area under the curve [77]. The proportion of these differences greater than or equal to the true observed
422 difference was used as the p -value. A significance level of 0.05 was used to reject the null hypothesis, H_0 : no
423 difference in mean area under the curve, in favor of our alternative hypothesis, H_1 : difference of mean area
424 under the curve.

425 Design of random forest model

426 A random forest model was built in python using the scikit learn module [47, 46]. Association statistics from
427 the ATAC-seq data generated in this study on A549 cells and additional ATAC-seq data downloaded from the
428 ENCODE project was used as input (see Table 1). As features in this random forest, the R^2 coefficient and
429 normalized mutual information were calculated between every pair of ATAC-seq experiments using WFpkm
430 counts, across ten kilobase pair, genomic bins and removing co-zero values. The comparison of each unique
431 pair of experiments (totaling 276) were discretized as (1) between independent ATAC-seq experiments in
432 different cell lines, (2) independent experiments using the same cell line, and (3) between true replicates.
433 The total number of comparisons distributed among these three classes was 213, 45, and 18 (respectively).
434 Given the over-representation of comparison between independent ATAC-seq experiments in different cell
435 lines, 39 of the 213 comparisons were chosen randomly to represent the total, unique comparisons between
436 experiments with unique cell lines. This down sampling resulted in 39, 45, and 18 comparisons between
437 independent experiments in different cell lines, independent experiments using the same cell line, and true
438 replicate experiments, respectively.

439 For the testing and training of the model, test and training sets of the classes defined above were selected
440 using a stratified, 40:60 split of the data. Additionally, ten-fold, stratified cross validation was used to train
441 and test the model [78]. A hundred estimators with the entropy selection criterion were used along with
442 default settings in the python random forest classifier function within scikit learn [46].

443 **Declarations**

444 **Ethics approval and consent to participate**

445 Not applicable

446 **Consent for publication**

447 Approved for public release; distribution is unlimited: LA-UR-23-24317

448 **Data availability**

449 All data and code associated with this manuscript (if not publicly available) is available upon request. Raw
450 sequence reads generated by this study on A549 samples are deposited and stored on NCBI's Sequence Read
451 Archive, with accession numbers SAMN35335737 – SAMN35335744. Scripts, code, and software used in
452 the statistical analysis and visualization are stored on GitHub: [https://github.com/cjr41/SLURPY/tree/
453 main/ATAC_SEQ_SIMULATION](https://github.com/cjr41/SLURPY/tree/main/ATAC_SEQ_SIMULATION)

454 **Competing interests**

455 The authors declare no competing interests.

456 **Authors' contributions**

457 The authors (with initials) CR, VV, VJ, NL, KYS, CRS, and SRS contributed to the overall experimental
458 design of this manuscript. VV and CRS provided materials and wrote experimental methods. VV prepared
459 experimental ATAC-seq data for cultured A549 cells. CR conducted analysis and produced visualizations.
460 CR, CRS, and SRS wrote the paper. All authors edited and provided comments on the text of the manuscript.

461 **Funding**

462 The work conducted within this paper was funded by the Los Alamos National Laboratory Directed Research
463 grant (20210082DR) awarded to SRS and KYS.

464 **Acknowledgements**

465 We would like to thank members of the Genomics and Bioanalytics Group at Los Alamos National Laboratory
466 for their helpful comments on this manuscript. Special thanks to Drs. Taehyung Kwon and Colin Kruse for
467 their specific and helpful suggestions on analyses. We would also like to acknowledge and thank the ENCODE
468 Consortium and the members of the Michael Snyder lab of Stanford, for generating the ATAC-seq data sets
469 used within this study.

470 **Tables**

Table 1: ATAC-seq Experiments Used, Mapped Reads, Peak Counts and FrIP Scores

Sample Title	Cell Line	Mapped Reads	MACS2 Peaks	FrIP	Source
A549 ₀₀₀	A549	259029456	201532	0.5898	ENCSR032RGS
A549 ₀₀₁	A549	329679445	194975	0.5994	ENCSR032RGS
A549 ₀₀₂	A549	211291691	206536	0.5596	ENCSR032RGS
A549 ₁₀₀	A549	23987725	110323	0.588	This study
A549 ₁₀₁	A549	22605005	81917	0.3404	This study
A549 ₁₀₂	A549	17618743	82496	0.3702	This study
A549 ₂₀₀	A549	35069198	90386	0.3515	This study
A549 ₂₀₁	A549	15377297	79933	0.4202	This study
A549 ₃₀₀	A549	42567716	130475	0.636	This study
A549 ₃₀₁	A549	28744542	107737	0.6391	This study
A549 ₃₀₂	A549	35836016	117087	0.6595	This study
GM12878 ₄₀₀	GM12878	46889870	114746	0.7159	ENCSR095QNB
GM12878 ₄₀₁	GM12878	49588811	134743	0.6452	ENCSR095QNB
HepG2 ₅₀₀	HepG2	48113686	173756	0.4257	ENCSR042AWH
HepG2 ₅₀₁	HepG2	48246610	135767	0.4605	ENCSR042AWH
IMR-90 ₆₀₀	IMR-90	47543633	178156	0.5363	ENCSR200OML
IMR-90 ₆₀₁	IMR-90	61359070	200216	0.6104	ENCSR200OML
K562 ₇₀₀	K562	48217636	178230	0.5112	ENCSR483RKN
K562 ₇₀₁	K562	52270533	176789	0.5196	ENCSR483RKN
RWPE2 ₈₀₀	RWPE2	55152003	166239	0.474	ENCSR080SNF
RWPE2 ₈₀₁	RWPE2	43166947	177496	0.4555	ENCSR080SNF
RWPE2 ₈₀₂	RWPE2	48162285	154758	0.4652	ENCSR080SNF
WTC11 ₉₀₀	WTC11	74558506	245677	0.5505	ENCSR541KFY
WTC11 ₉₀₁	WTC11	79335328	277824	0.5732	ENCSR541KFY

Table 2: Mean Area Under the Curve Across Simulations

Statistic	Mean (95% CI)	Mean (95% CI) – Co-zeros removed	p-value ^a	σ^2 ^b
Top-Down Correlation				
Pearson R	0.6881 (0.6860 – 0.6906)	0.6872 (0.6850 – 0.6895)	0.635	-
R^2	0.8284 (0.8237 – 0.8335)	0.6965 (0.6946 – 0.6984)	0.0	0.0201
Spearman ρ	0.7026 (0.6951 – 0.7102)	0.5346 (0.5324 – 0.5368)	0.0	0.0329
Kendall τ	0.9140 (0.9118 – 0.9162)	0.6686 (0.6665 – 0.6705)	0.0	0.0136
Kendall W	0.9096 (0.9074 – 0.9120)	0.6673 (0.6654 – 0.6691)	0.0	-
Normalized Mutual Information	0.9570 (0.9559 – 0.9581)	0.8343 (0.8333 – 0.8353)	0.0	-
	0.8197 (0.8153 – 0.8241)	0.5055 (0.5045 – 0.5065)	0.0	0.016

^a The p -value represents the test of differences in mean AUC after removal of co-zeros.

^b Variation values were calculated during analysis of data from true ATAC-seq experiments.

471 Figures

21

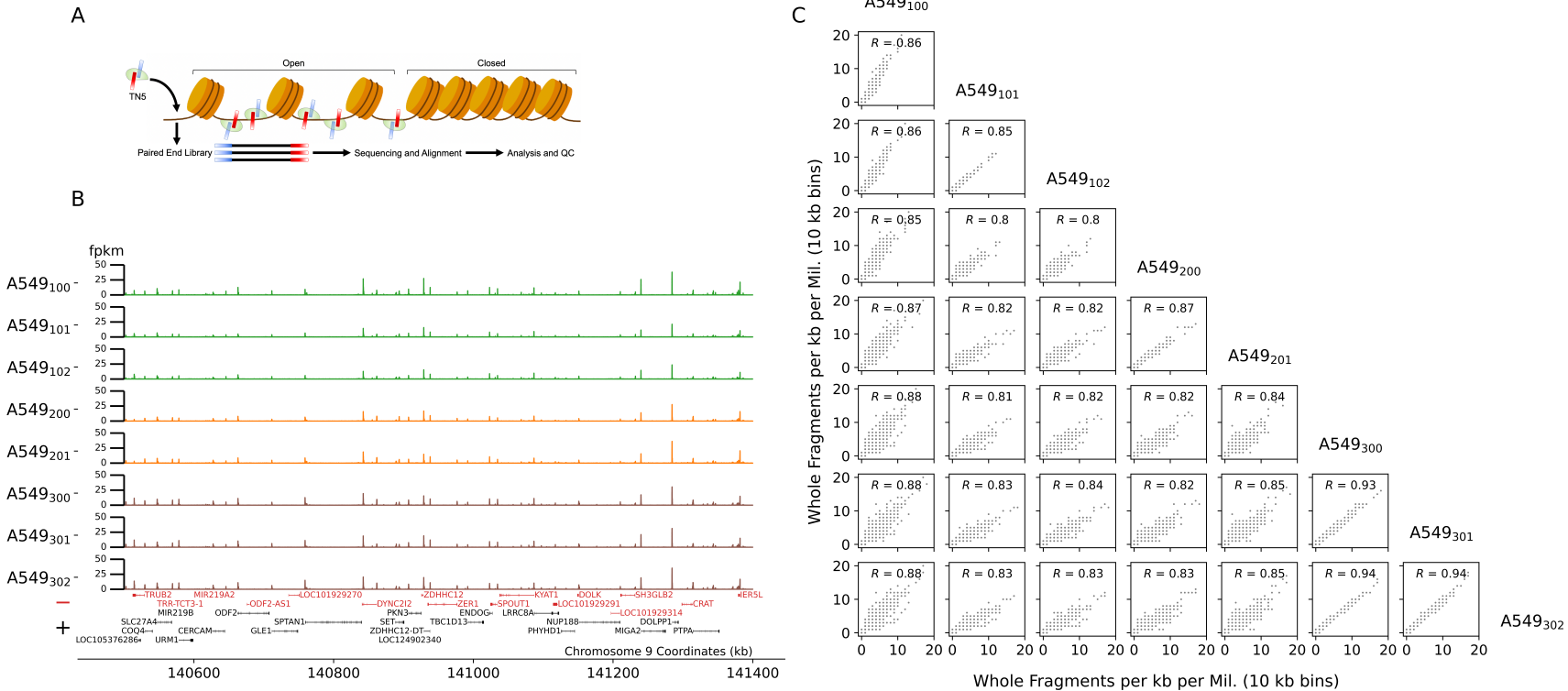


Figure 1: ATAC-seq profiles of chromosome 9 from A549 cells. **A:** TN5 binds to open chromatin, cutting DNA and adding primers to generate a paired-end sequencing library. **B:** A549, ATAC-seq replicates along chromosome 9. Samples were generated using fresh cells (green) and previously cryo-preserved cell cultures (orange and brown). Positively (black) and negatively oriented genes are annotated along the bottom. **C:** Pair-wise, bi-variate scatter plots of whole fragments per kb per million values (x- and y-axis) using 10 kb genomic bins between A549, ATAC-seq replicates. Sample names are annotated along the diagonal. Pair-wise Pearson's correlation statistic is annotated within subplots.

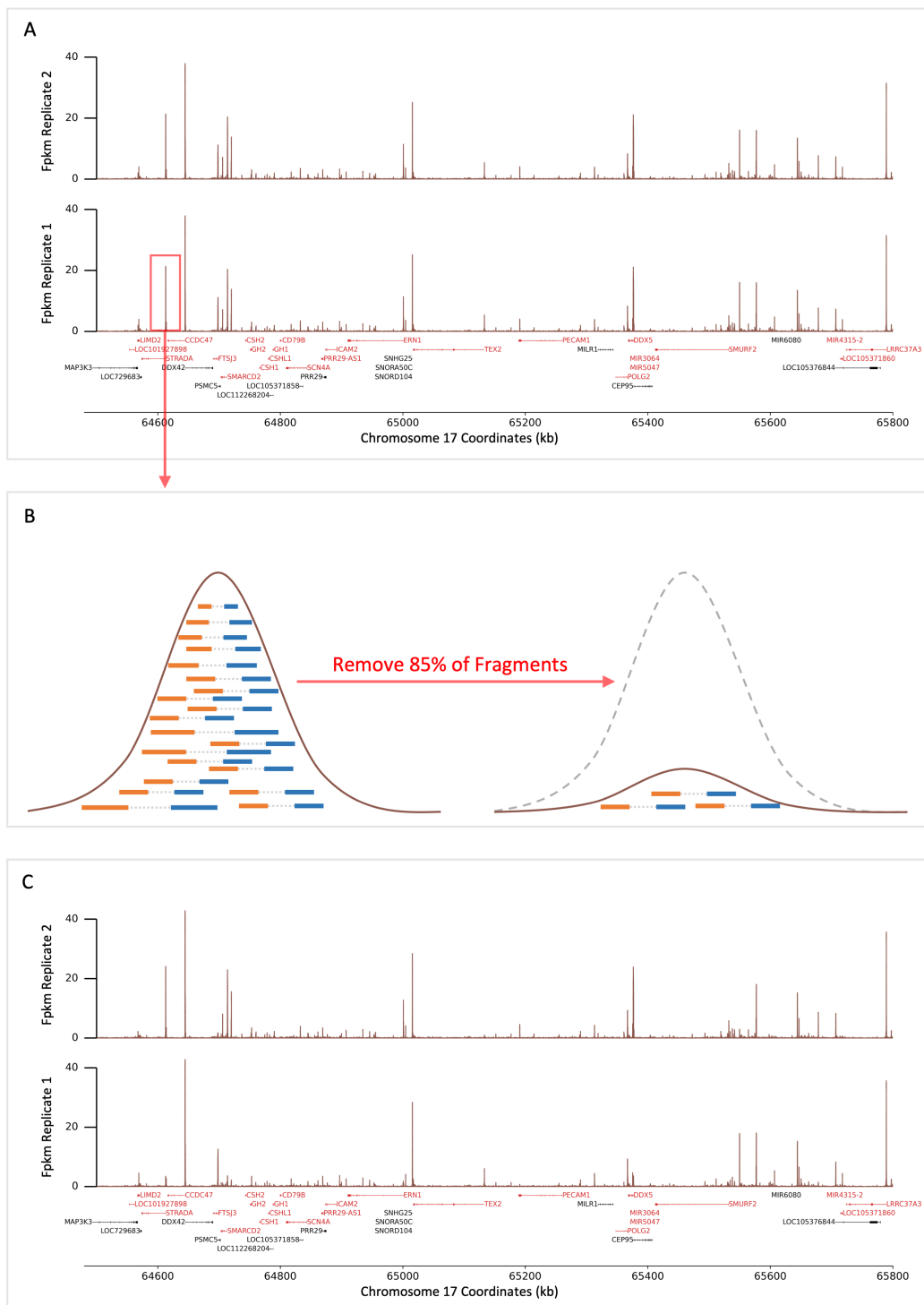


Figure 2: Synthetic replicate generation via peak down-sampling. **A:** An example region along chromosome 17 of true, A549 ATAC-seq data. Real ATAC-seq signal (brown lines) is used to initialize two synthetic replicates. Red and black horizontal bodies depict negatively and positively oriented genes, respectively. **B:** A portion of the genome-wide significant peaks (ranging from 0 - 1) are chosen randomly between the two synthetic replicates. Within one of the replicates, 85% of paired reads (blue and orange rectangles connected by grey dotted line) are removed to down-sample signal within that locus. **C:** Example of two synthetic replicates with a known portion of peaks varying between them.

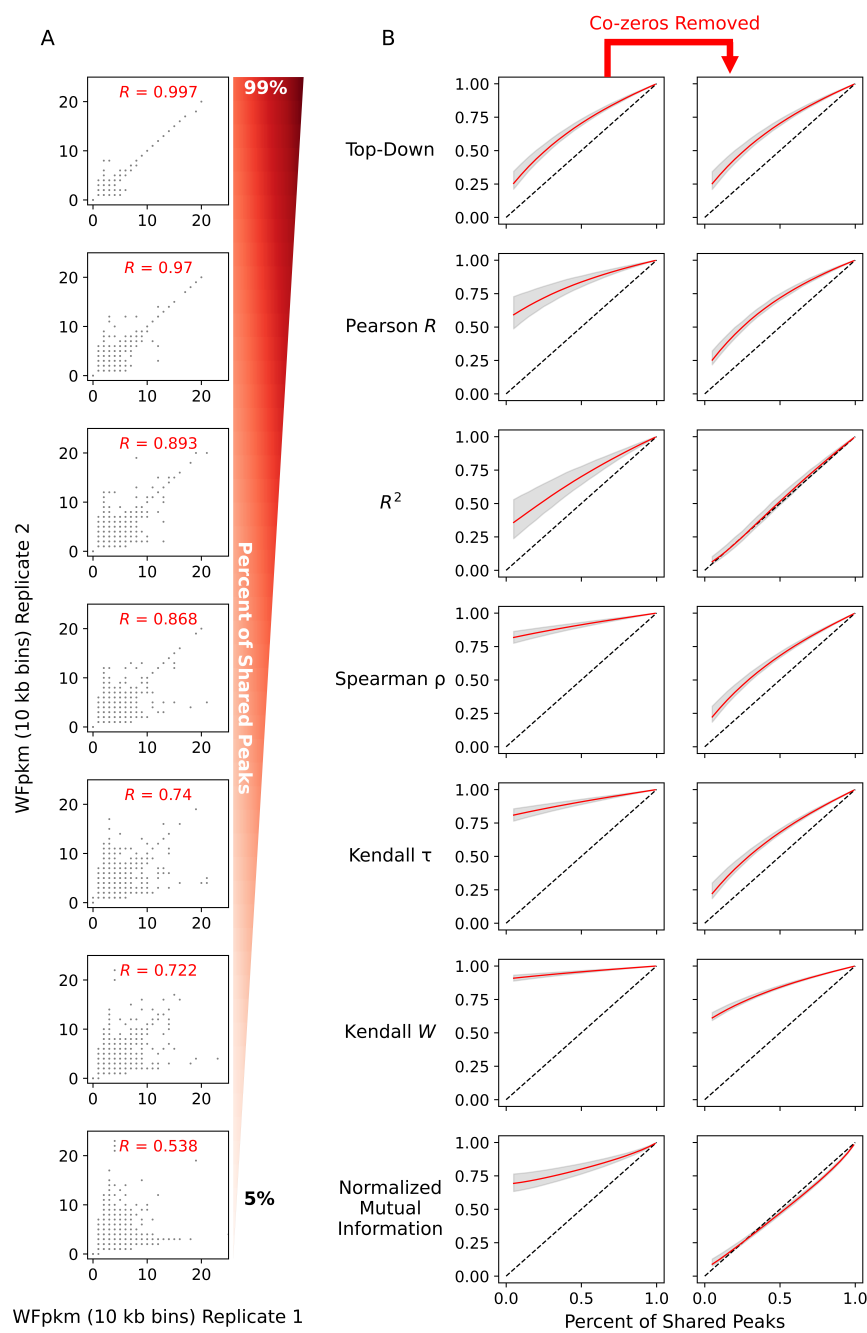


Figure 3: Synthetic replicate bivariate plots and statistical profiles. **A:** Scatter plots displaying counts per genomic bin (10 kb in size) of whole fragments per kilobase per million between two synthetic replicates (x- and y-axis) generated in process Figure 2A – C. The percentage of shared peaks decreases between the two simulated replicates from top to bottom. **B:** Correlation and association values (y-axis) as a function of percentage of shared peaks between synthetic replicates (x-axis). Red and grey curves depict the mean and 95% CI (respectively) values across simulations. A grey, dashed line marks a one-to-one relationship between the x- and y-axis. Left and right columns display change in values as a function of removing co-zeros.

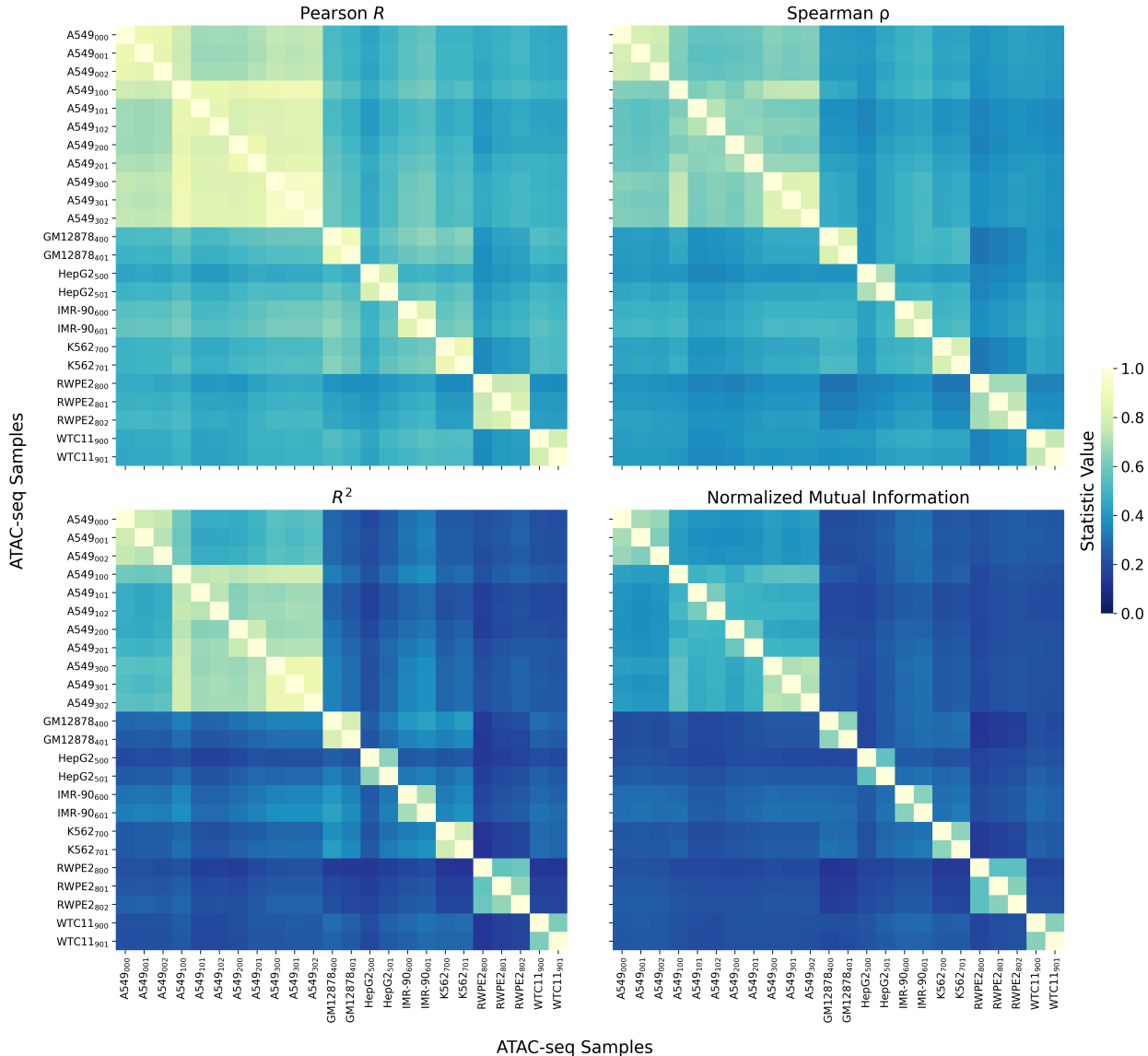


Figure 4: Correlation and association statistics across ATAC-seq experiments. From top-to-bottom, left-to-right, the Person's R , Spearman's ρ , R^2 coefficient, and normalized mutual information across ATAC-seq replicates from the ENCODE project and ATAC-seq experiments on A549 cells generated in this study.

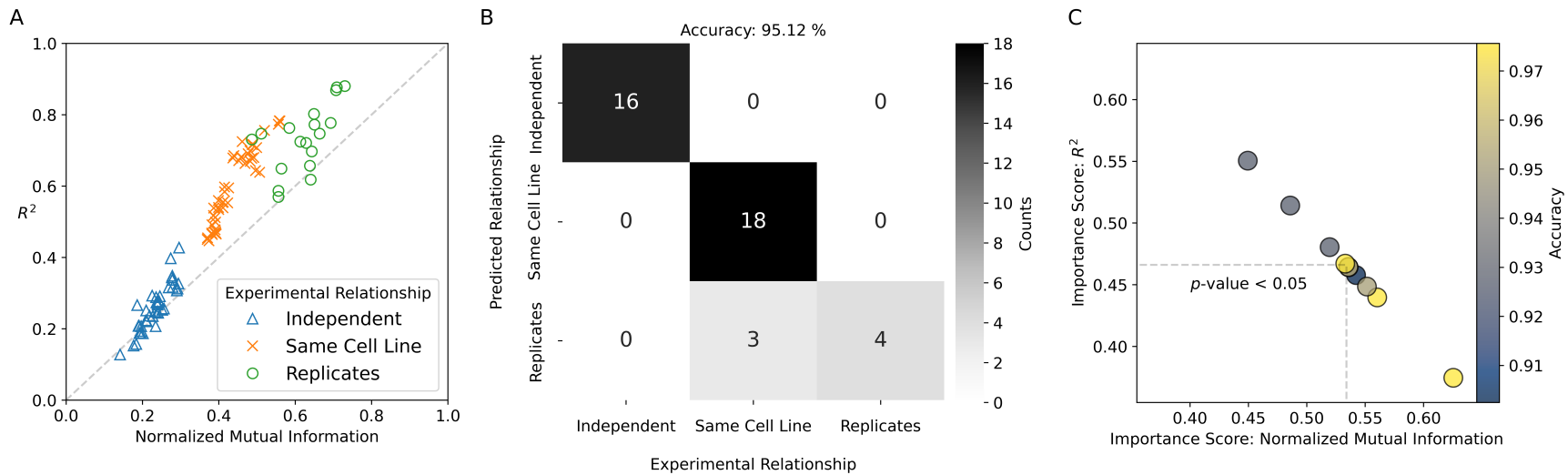


Figure 5: Random forest prediction of experimental relationships. **A:** The coefficient of determination (R^2) versus the normalized mutual information (y- and x-axis, respectively) calculated on binned counts of WFpkm between ATAC-seq experiments. Blue triangles, orange Xs, and green circles mark comparisons between independent experiments, independent experiments using the same cell line, and true experimental replicates, respectively. **B:** Example confusion matrix from a random forest model using R^2 and normalized mutual information as features to predict experimental relationships (y-axis) presented in **A** (x-axis). The confusion matrix depicts results of model on a hold-out set (40% of data, accuracy = 95.12%). Light to dark colors depict the number of counts per class. **C:** Bi-variate plot displaying the change of paired importance scores from ten-fold cross validation between the normalized mutual information (x-axis) and R^2 (y-axis) features. Dashed lines depict the uni-variate means of the normalized mutual information and R^2 scores. Blue and yellow colors depict the level of accuracy for each fold.

472 Supplementary Materials

473 Additional File 1

- 474 • Title: Statistical_profiles_Simulation_0.50.png
- 475 • File Format: png
- 476 • Description: Correlation and association values (y-axis) as a function of percentage of shared peaks
477 between synthetic replicates (x-axis). Red and grey curves depict the mean and 95% CI (respectively)
478 values across simulations. A grey, dashed line marks a one-to-one relationship between the x- and
479 y-axis. Left and right columns display change in values as a function of removing co-zeros. Results are
480 from simulations with 50% paired reads within selected peaks removed.

481 Additional File 2

- 482 • Title: Statistical_profiles_Simulation_0.95.png
- 483 • File Format: png
- 484 • Description: Correlation and association values (y-axis) as a function of percentage of shared peaks
485 between synthetic replicates (x-axis). Red and grey curves depict the mean and 95% CI (respectively)
486 values across simulations. A grey, dashed line marks a one-to-one relationship between the x- and
487 y-axis. Left and right columns display change in values as a function of removing co-zeros. Results are
488 from simulations with 95% paired reads within selected peaks removed.

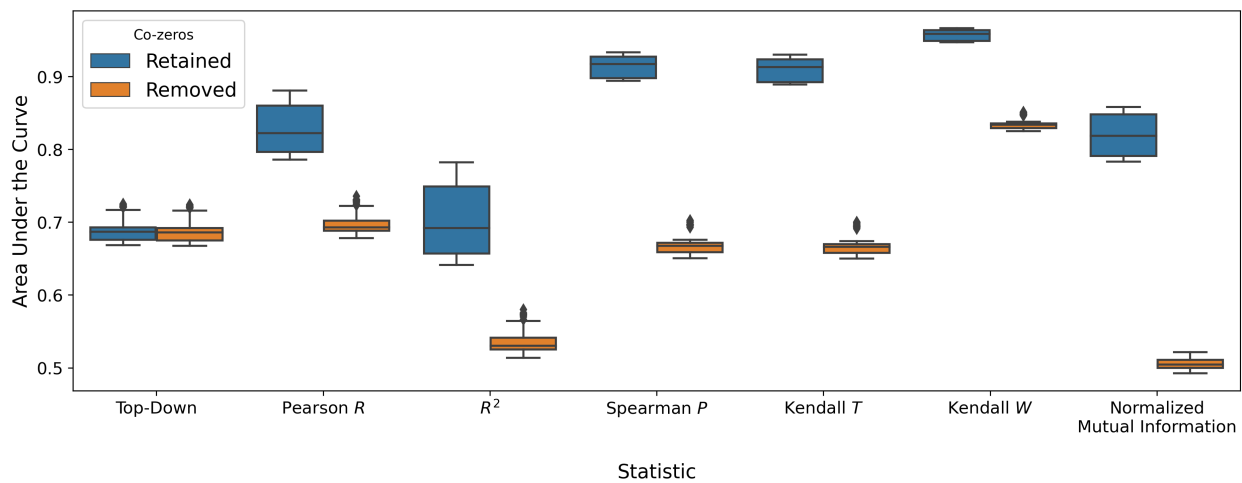


Figure S1: Boxplots displaying the area under the curve (y-axis) across statistics (x-axis) with co-zeros retained and removed from analysis (blue and orange boxes, respectively).

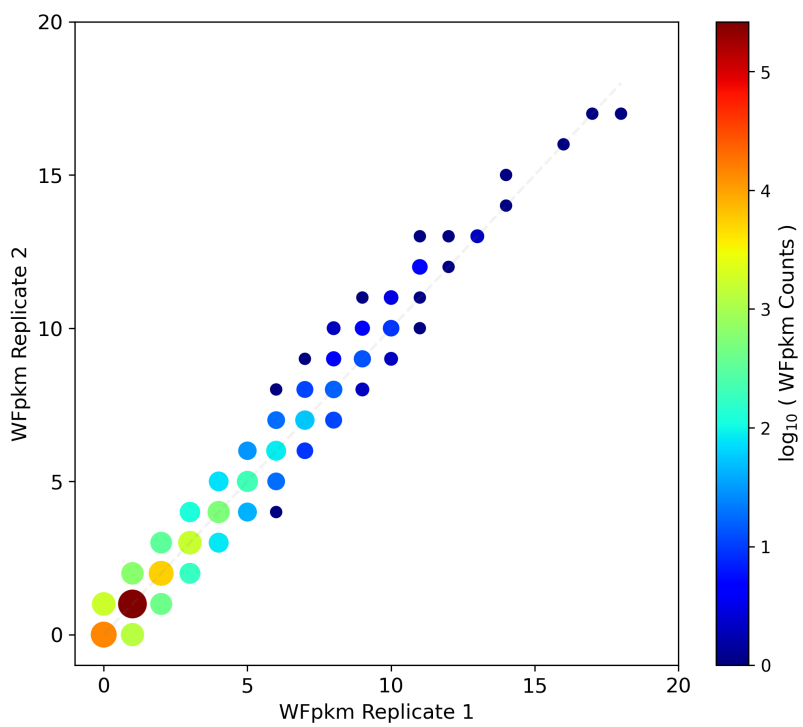


Figure S2: Bi-variate plot of WFpkm counts (across 10 kb genomic bins) between replicates of real, A549 ATAC-seq experiments. Dark red to blue colors and marker size designate the density (log₁₀ (WFpkm counts)) of counts between replicates. Co-zero values appear as an orange dot in lower left corner. A dashed grey line represents a one-to-one relationship between the two replicates.

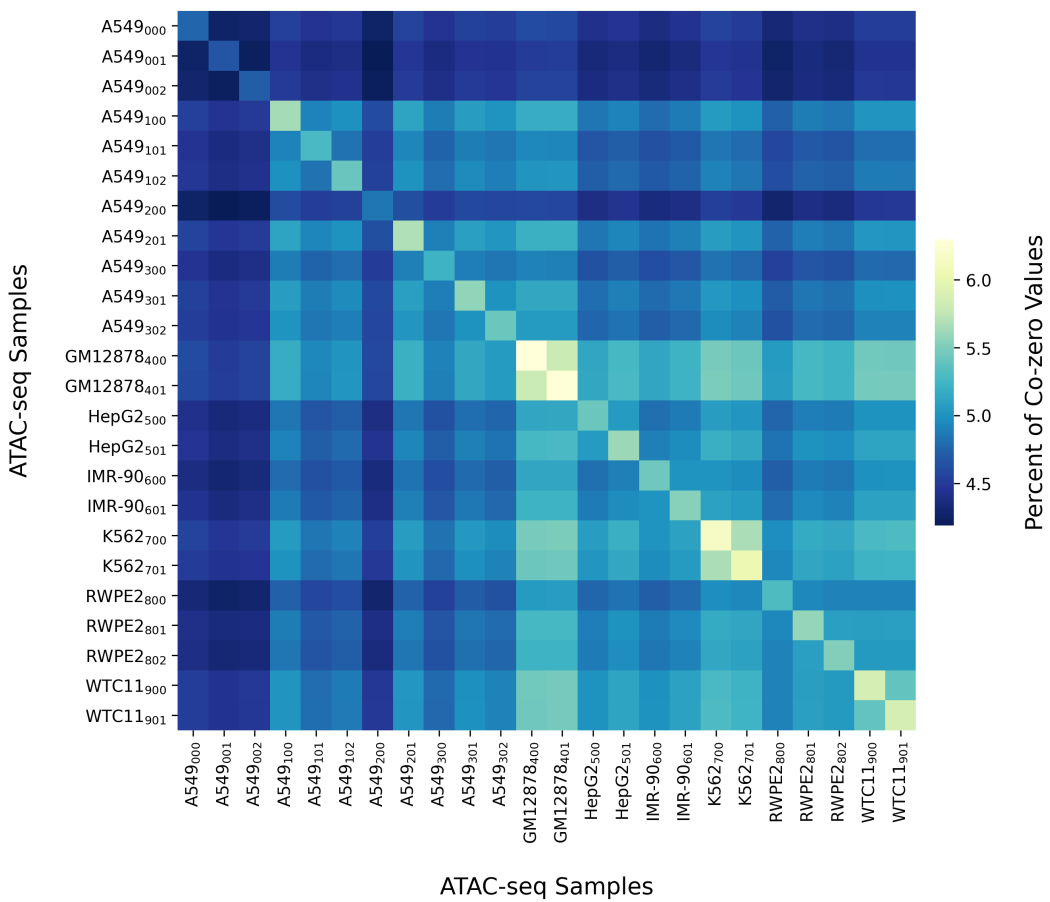


Figure S3: The percent of co-zero values in bi-variate WFpkm distributions between real ATAC-seq experiments. Sample names are annotated along the x- and y-axis.

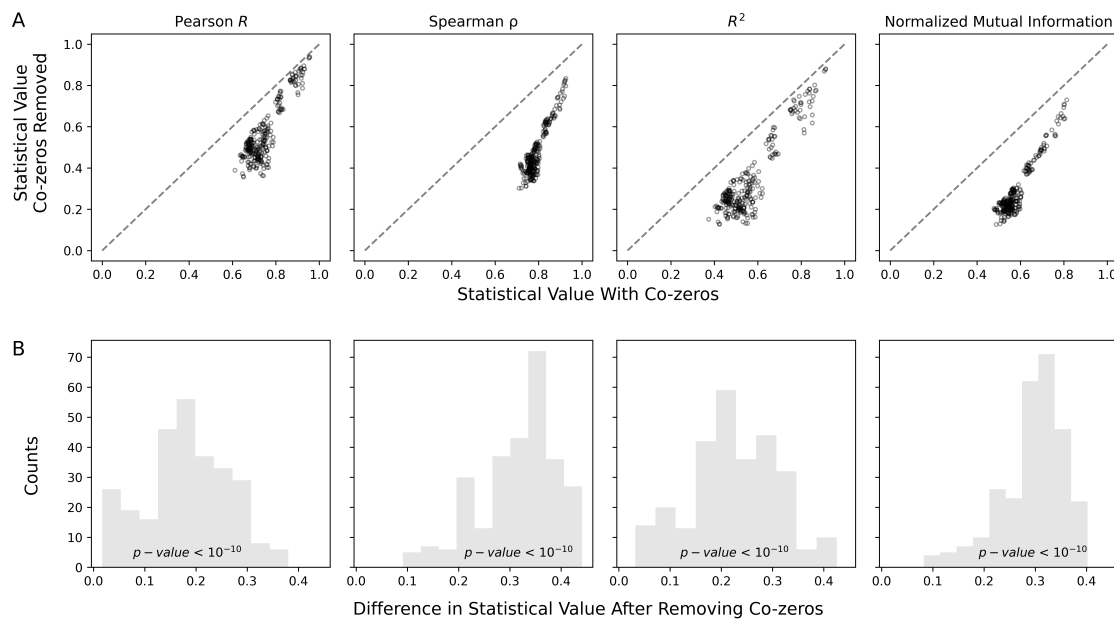


Figure S4: The effect of removing co-zeros from analysis on ATAC-seq experiments from the ENCODE project. **A** Shift in the estimates of correlation and association before (x-axis) and after (y-axis) removing co-zeros from analysis for the Pearson's R , the Spearman's ρ , R^2 coefficient, and normalized mutual information, left to right respectively. A dashed line denotes a one-to-one relationship. **B** The pair-wise difference in correlation and association metrics from estimates before and after removing co-zeros.

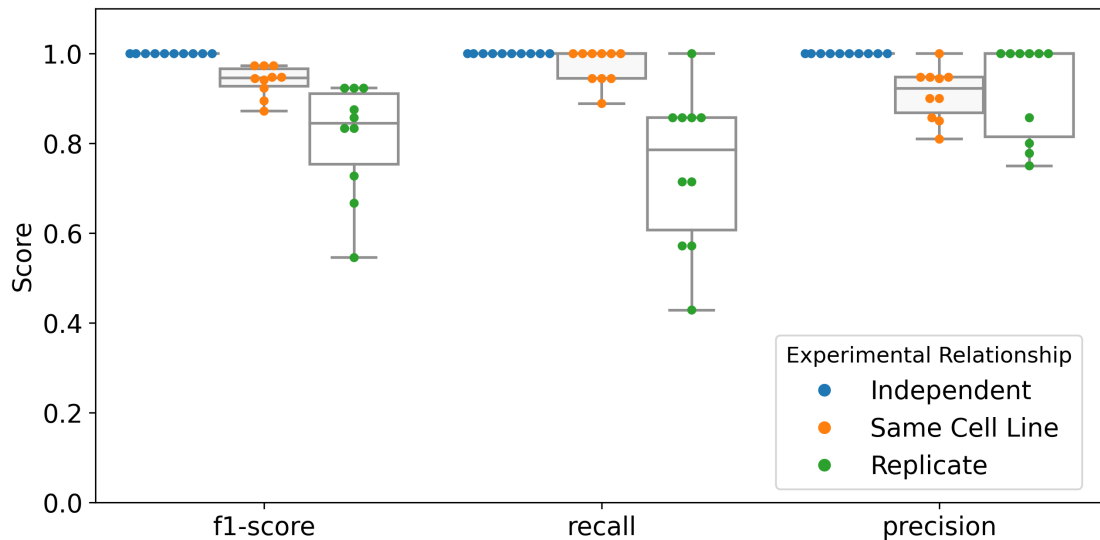


Figure S5: The f1-scores, recall, and precision of the random forest model with ten-fold, stratified cross validation. Blue, orange, and green colors denote experimental relationship class.

Table S1: Read Counts of ATAC-seq Experiments

Sample Title	Cell Line	Total Reads	Mapped Reads	Not Used	mtDNA	Duplicates	Un-mapped	Low Quality Reads	Replicate Name	Source
A549 ₀₀₀	A549	341325836	259029456	21246814	12009324	46948944	408486	1682812	ENCLB404SKN	ENCSR032RGS
A549 ₀₀₁	A549	442074976	329679445	27536117	15475857	66338506	506856	2538195	ENCLB605LCC	ENCSR032RGS
A549 ₀₀₂	A549	277970512	211291691	18456829	11170486	35323112	343051	1385343	ENCLB817BKI	ENCSR032RGS
A549 ₁₀₀	A549	65405524	23987725	2973344	33653170	3093813	48906	1648566	2501_001	This study
A549 ₁₀₁	A549	84816540	22605005	2595465	55231224	2481489	32350	1871007	2501_002	This study
A549 ₁₀₂	A549	64084756	17618743	2122339	40809830	1979951	67472	1486421	2501_003	This study
A549 ₂₀₀	A549	133625408	35069198	4386111	86279921	4418826	31955	3439397	2501_007	This study
A549 ₂₀₁	A549	69273610	15377297	1834370	48556785	1780806	27699	1696653	2501_008	This study
A549 ₃₀₀	A549	86963986	42567716	4788405	31620108	5703777	121028	2162952	2501_018	This study
A549 ₃₀₁	A549	84297712	28744542	3582876	44737775	5400961	118620	1712938	2501_019	This study
A549 ₃₀₂	A549	97877188	35836016	4491769	49816243	5663997	42546	2026617	2501_020	This study
GM12878 ₄₀₀	GM12878	76479882	46889870	4260513	11245729	12635046	252057	1196667	ENCLB584REF	ENCSR095QNB
GM12878 ₄₀₁	GM12878	69456510	49588811	4319318	7334534	6740176	186878	1286793	ENCLB907YRF	ENCSR095QNB
HepG2 ₅₀₀	HepG2	76077306	48113686	6037783	8348893	11668633	235020	1673291	ENCLB074EQT	ENCSR042AWH
HepG2 ₅₀₁	HepG2	88838406	48246610	6580203	19207768	12021756	605060	2177009	ENCLB324GIU	ENCSR042AWH
IMR-90 ₆₀₀	IMR-90	84117916	47543633	11830808	8448694	9559287	5990188	745306	ENCLB432QLN	ENCSR200OML
IMR-90 ₆₀₁	IMR-90	95034796	61359070	6202820	14378540	10233756	1872742	987868	ENCLB937FOM	ENCSR200OML
K562 ₇₀₀	K562	78745422	48217636	6777147	10759718	10705486	91659	2193776	ENCLB758GEG	ENCSR483RKN
K562 ₇₀₁	K562	83982064	52270533	6752478	10447009	12175330	162811	2173903	ENCLB918NXF	ENCSR483RKN
RWPE2 ₈₀₀	RWPE2	67263926	55152003	6718663	753542	2685741	286519	1667458	ENCLB293SLX	ENCSR080SNF
RWPE2 ₈₀₁	RWPE2	53441754	43166947	5244472	1277887	2088775	323207	1340466	ENCLB734LAL	ENCSR080SNF
RWPE2 ₈₀₂	RWPE2	60212304	48162285	5946340	1888964	2288274	331284	1595157	ENCLB984XHJ	ENCSR080SNF
WTC11 ₉₀₀	WTC11	115952320	74558506	7218516	7595855	21538753	4422396	618294	ENCLB621FEI	ENCSR541KFY
WTC11 ₉₀₁	WTC11	127343084	79335328	7889715	9553155	24757738	5028262	778886	ENCLB715JYV	ENCSR541KFY

489 References

490 [1] Barski A, Cuddapah S, Cui K, Roh TY, Schones DE, Wang Z, et al. High-resolution profiling of histone
491 methylation in the human genome. *Cell*. 2007;129(4):823–837.

492 [2] Barski A, Zhao K. Genomic location analysis by ChIP-Seq. *Journal of cellular biochemistry*.
493 2009;107(1):11–18.

494 [3] Park PJ. ChIP-seq: advantages and challenges of a maturing technology. *Nature reviews genetics*.
495 2009;10(10):669–680.

496 [4] Buenrostro JD, Wu B, Chang HY, Greenleaf WJ. ATAC-seq: a method for assaying chromatin accessibility
497 genome-wide. *Current protocols in molecular biology*. 2015;109(1):21–29.

498 [5] Thorvaldsdóttir H, Robinson JT, Mesirov JP. Integrative Genomics Viewer (IGV): high-performance
499 genomics data visualization and exploration. *Briefings in bioinformatics*. 2013;14(2):178–192.

500 [6] Zhang Y, Liu T, Meyer CA, Eeckhoute J, Johnson DS, Bernstein BE, et al. Model-based analysis of
501 ChIP-Seq (MACS). *Genome biology*. 2008;9(9):1–9.

502 [7] Heinz S, Benner C, Spann N, Bertolino E, Lin YC, Laslo P, et al. Simple combinations of lineage-
503 determining transcription factors prime cis-regulatory elements required for macrophage and B cell
504 identities. *Molecular cell*. 2010;38(4):576–589.

505 [8] Landt SG, Marinov GK, Kundaje A, Kheradpour P, Pauli F, Batzoglou S, et al. ChIP-seq guidelines
506 and practices of the ENCODE and modENCODE consortia. *Genome research*. 2012;22(9):1813–1831.

507 [9] Oh D, Strattan JS, Hur JK, Bento J, Urban AE, Song G, et al. CNN-Peaks: ChIP-Seq peak detection
508 pipeline using convolutional neural networks that imitate human visual inspection. *Scientific reports*.
509 2020;10(1):7933.

510 [10] Yan F, Powell DR, Curtis DJ, Wong NC. From reads to insight: a hitchhiker's guide to ATAC-seq data
511 analysis. *Genome biology*. 2020;21:1–16.

512 [11] Consortium EP, et al. An integrated encyclopedia of DNA elements in the human genome. *Nature*.
513 2012;489(7414):57.

514 [12] Luo Y, Hitz BC, Gabdank I, Hilton JA, Kagda MS, Lam B, et al. New developments on the Encyclopedia
515 of DNA Elements (ENCODE) data portal. *Nucleic acids research*. 2020;48(D1):D882–D889.

516 [13] Ramírez F, Dündar F, Diehl S, Grüning BA, Manke T. deepTools: a flexible platform for exploring
517 deep-sequencing data. *Nucleic acids research*. 2014;42(W1):W187–W191.

518 [14] Grandi FC, Modi H, Kampman L, Corces MR. Chromatin accessibility profiling by ATAC-seq. *Nature
519 Protocols*. 2022;17(6):1518–1552.

520 [15] Sahinyan K, Blackburn DM, Simon MM, Lazure F, Kwan T, Bourque G, et al. Application of ATAC-Seq
521 for genome-wide analysis of the chromatin state at single myofiber resolution. *Elife*. 2022;11:e72792.

522 [16] Zhao Y, Li MC, Konaté MM, Chen L, Das B, Karlovich C, et al. TPM, FPKM, or normalized counts?
523 A comparative study of quantification measures for the analysis of RNA-seq data from the NCI patient-
524 derived models repository. *Journal of translational medicine*. 2021;19(1):1–15.

525 [17] Schober P, Boer C, Schwarte LA. Correlation coefficients: appropriate use and interpretation. *Anesthesia
526 & analgesia*. 2018;126(5):1763–1768.

527 [18] Milani P, Escalante-Chong R, Shelley BC, Patel-Murray NL, Xin X, Adam M, et al. Cell freezing
528 protocol suitable for ATAC-Seq on motor neurons derived from human induced pluripotent stem cells.
529 *Scientific reports*. 2016;6(1):1–10.

530 [19] Shan X, Roberts C, Lan Y, Percec I. Age alters chromatin structure and expression of SUMO proteins
531 under stress conditions in human adipose-derived stem cells. *Scientific reports*. 2018;8(1):11502.

532 [20] Corces MR, Granja JM, Shams S, Louie BH, Seoane JA, Zhou W, et al. The chromatin accessibility
533 landscape of primary human cancers. *Science*. 2018;362(6413):eaav1898.

534 [21] Halstead M, Kern C, Saelao P, Chanthavixay G, Wang Y, Delany M, et al. Systematic alteration
535 of ATAC-seq for profiling open chromatin in cryopreserved nuclei preparations from livestock tissues.
536 *Scientific reports*. 2020;10(1):1–12.

537 [22] Fang R, Preissl S, Li Y, Hou X, Lucero J, Wang X, et al. Comprehensive analysis of single cell ATAC-seq
538 data with SnapATAC. *Nature communications*. 2021;12(1):1337.

539 [23] Wong YY, Harbison JE, Hope CM, Gundsambuu B, Brown KA, Wong SW, et al. Parallel recovery of
540 chromatin accessibility and gene expression dynamics from frozen human regulatory T cells. *Scientific
541 Reports*. 2023;13(1):5506.

542 [24] Lynch M, Walsh B, et al. Genetics and analysis of quantitative traits. vol. 1. Sinauer Sunderland, MA;
543 1998.

544 [25] Conesa A, Madrigal P, Tarazona S, Gomez-Cabrero D, Cervera A, McPherson A, et al. A survey of
545 best practices for RNA-seq data analysis. *Genome biology*. 2016;17(1):1–19.

546 [26] Yan KK, Yardimci GG, Yan C, Noble WS, Gerstein M. HiC-spector: a matrix library for spectral and
547 reproducibility analysis of Hi-C contact maps. *Bioinformatics*. 2017;33(14):2199–2201.

548 [27] Yang T, Zhang F, Yardimci GG, Song F, Hardison RC, Noble WS, et al. HiCRep: assessing
549 the reproducibility of Hi-C data using a stratum-adjusted correlation coefficient. *Genome research*.
550 2017;27(11):1939–1949.

551 [28] Roth C, Sun S, Billmyre RB, Heitman J, Magwene PM. A high-resolution map of meiotic recombination
552 in *Cryptococcus deneoformans* demonstrates decreased recombination in unisexual reproduction.
553 *Genetics*. 2018;209(2):567–578.

554 [29] Stansfield JC, Cresswell KG, Vladimirov VI, Dozmorov MG. HiCcompare: an R-package for joint
555 normalization and comparison of HI-C datasets. *BMC bioinformatics*. 2018;19(1):1–10.

556 [30] Yardimci GG, Ozadam H, Sauria ME, Ursu O, Yan KK, Yang T, et al. Measuring the reproducibility
557 and quality of Hi-C data. *Genome biology*. 2019;20(1):1–19.

558 [31] Ramírez F, Ryan DP, Grüning B, Bhardwaj V, Kilpert F, Richter AS, et al. deepTools2: a next
559 generation web server for deep-sequencing data analysis. *Nucleic acids research*. 2016;44(W1):W160–
560 W165.

561 [32] Ramírez F, Bhardwaj V, Arrigoni L, Lam KC, Grüning BA, Villaveces J, et al. High-resolution TADs
562 reveal DNA sequences underlying genome organization in flies. *Nature communications*. 2018;9(1):189.

563 [33] Wolff J, Bhardwaj V, Nothjunge S, Richard G, Renschler G, Gilsbach R, et al. Galaxy HiCExplorer: a
564 web server for reproducible Hi-C data analysis, quality control and visualization. *Nucleic acids research*.
565 2018;46(W1):W11–W16.

566 [34] Wolff J, Rabbani L, Gilsbach R, Richard G, Manke T, Backofen R, et al. Galaxy HiCExplorer 3: a
567 web server for reproducible Hi-C, capture Hi-C and single-cell Hi-C data analysis, quality control and
568 visualization. *Nucleic acids research*. 2020;48(W1):W177–W184.

569 [35] Nimon KF. Statistical assumptions of substantive analyses across the general linear model: a mini-
570 review. *Frontiers in psychology*. 2012;3:322.

571 [36] Silverman JD, Roche K, Mukherjee S, David LA. Naught all zeros in sequence count data are the same.
572 *Computational and structural biotechnology journal*. 2020;18:2789–2798.

573 [37] Student. Probable error of a correlation coefficient. *Biometrika*. 1908;6(2-3):302–310.

574 [38] Fisher R. *Statistical Methods for Research Workers* Oliver and Boyd, London. Reprinted in *Statistical*
575 *Methods, Experimental Design and Scientific Inference*; 1925.

576 [39] Kowalski CJ. On the effects of non-normality on the distribution of the sample product-moment correla-
577 *tion coefficient. Journal of the Royal Statistical Society: Series C (Applied Statistics)*. 1972;21(1):1–12.

578 [40] Kokoska S, Zwillinger D. *CRC standard probability and statistics tables and formulae*. Crc Press; 2000.

579 [41] Kendall M. *Rank correlation methods* 4th edition charles griffin. High Wycombe, Bucks. 1970;;

580 [42] Noether GE. *Elements of nonparametric statistics. Elements of Nonparametric Statistics*. 1967;;

581 [43] Arndt S, Turvey C, Andreasen NC. Correlating and predicting psychiatric symptom ratings: Spearmans
582 r versus Kendalls tau correlation. *Journal of psychiatric research*. 1999;33(2):97–104.

583 [44] Xu W, Hou Y, Hung Y, Zou Y. A comparative analysis of Spearman's rho and Kendall's tau in normal
584 and contaminated normal models. *Signal Processing*. 2013;93(1):261–276.

585 [45] Cover TM. *Elements of information theory*. John Wiley & Sons; 1999.

586 [46] Pedregosa F, Varoquaux G, Gramfort A, Michel V, Thirion B, Grisel O, et al. Scikit-learn: Machine
587 Learning in Python. *Journal of Machine Learning Research*. 2011;12:2825–2830.

588 [47] Boulesteix AL, Janitza S, Kruppa J, König IR. Overview of random forest methodology and practical
589 guidance with emphasis on computational biology and bioinformatics. *Wiley Interdisciplinary Reviews: Data
590 Mining and Knowledge Discovery*. 2012;2(6):493–507.

591 [48] Iman RL, Conover W. A measure of top-down correlation. *Technometrics*. 1987;29(3):351–357.

592 [49] Fitzgerald T, Jones A, Engelhardt BE. A Poisson reduced-rank regression model for association mapping
593 in sequencing data. *BMC bioinformatics*. 2022;23(1):1–22.

594 [50] Kendall MG, Smith BB. The problem of m rankings. *The annals of mathematical statistics*.
595 1939;10(3):275–287.

596 [51] Burnham KP, Anderson DR, Burnham KP, Anderson DR. *Practical use of the information-theoretic
597 approach*. Springer; 1998.

598 [52] Varadan V, Miller III DM, Anastassiou D. Computational inference of the molecular logic for synaptic
599 connectivity in *C. elegans*. *Bioinformatics*. 2006;22(14):e497–e506.

600 [53] Anastassiou D. Computational analysis of the synergy among multiple interacting genes. *Molecular
601 systems biology*. 2007;3(1):83.

602 [54] Hu T, Chen Y, Kiralis JW, Collins RL, Wejse C, Sirugo G, et al. An information-gain approach to
603 detecting three-way epistatic interactions in genetic association studies. *Journal of the American Medical
604 Informatics Association*. 2013;20(4):630–636.

605 [55] Budden DM, Crampin EJ. Information theoretic approaches for inference of biological networks from
606 continuous-valued data. *BMC systems biology*. 2016;10(1):1–7.

607 [56] Roth C, Murray D, Scott A, Fu C, Averette AF, Sun S, et al. Pleiotropy and epistasis within
608 and between signaling pathways defines the genetic architecture of fungal virulence. *PLoS Genetics*.
609 2021;17(1):e1009313.

610 [57] Sun S, Roth C, Floyd Averette A, Magwene PM, Heitman J. Epistatic genetic interactions govern
611 morphogenesis during sexual reproduction and infection in a global human fungal pathogen. *Proceedings
612 of the National Academy of Sciences*. 2022;119(8):e2122293119.

613 [58] Chen H, Lareau C, Andreani T, Vinyard ME, Garcia SP, Clement K, et al. Assessment of computational
614 methods for the analysis of single-cell ATAC-seq data. *Genome biology*. 2019;20(1):1–25.

615 [59] Xu Y, Das P, McCord RP. SMILE: mutual information learning for integration of single-cell omics data.
616 *Bioinformatics*. 2022;38(2):476–486.

617 [60] Love MI, Huber W, Anders S. Moderated estimation of fold change and dispersion for RNA-seq data
618 with DESeq2. *Genome biology*. 2014;15(12):1–21.

619 [61] Stephens ZD, Hudson ME, Mainzer LS, Taschuk M, Weber MR, Iyer RK. Simulating next-generation
620 sequencing datasets from empirical mutation and sequencing models. *PloS one*. 2016;11(11):e0167047.

621 [62] Navidi Z, Zhang L, Wang B. simATAC: a single-cell ATAC-seq simulation framework. *Genome biology*.
622 2021;22:1–16.

623 [63] Giard DJ, Aaronson SA, Todaro GJ, Arnstein P, Kersey JH, Dosik H, et al. In vitro cultivation of
624 human tumors: establishment of cell lines derived from a series of solid tumors. *Journal of the National
625 Cancer Institute*. 1973;51(5):1417–1423.

626 [64] Foster KA, Oster CG, Mayer MM, Avery ML, Audus KL. Characterization of the A549 cell line as a type
627 II pulmonary epithelial cell model for drug metabolism. *Experimental cell research*. 1998;243(2):359–366.

628 [65] Peng KJ, Wang JH, Su WT, Wang XC, Yang FT, Nie WH, et al. Characterization of two human lung
629 adenocarcinoma cell lines by reciprocal chromosome painting. *Dongwuxue Yanjiu*. 2010;31(2):113–21.

630 [66] Chen S, Zhou, Y., Chen, Y., and Gu, J.(2018). Fastp: an Ultra-fast All-In-One FASTQ Preprocessor.
631 *Bioinformatics*. 2018;34(17):i884–i890.

632 [67] Nurk S, Koren S, Rhie A, Rautiainen M, Bzikadze AV, Mikheenko A, et al. The complete sequence of
633 a human genome. *Science*. 2022;376(6588):44–53.

634 [68] Li H, Durbin R. Fast and accurate short read alignment with Burrows–Wheeler transform. *bioinfor-
635 matics*. 2009;25(14):1754–1760.

636 [69] Faust GG, Hall IM. SAMBLASTER: fast duplicate marking and structural variant read extraction.
637 *Bioinformatics*. 2014;30(17):2503–2505.

638 [70] Consortium EP. A user’s guide to the encyclopedia of DNA elements (ENCODE). *PLoS biology*.
639 2011;9(4):e1001046.

640 [71] Feng J, Liu T, Qin B, Zhang Y, Liu XS. Identifying ChIP-seq enrichment using MACS. *Nature protocols*.
641 2012;7(9):1728–1740.

642 [72] Li H, Handsaker B, Wysoker A, Fennell T, Ruan J, Homer N, et al. The sequence alignment/map
643 format and SAMtools. *Bioinformatics*. 2009;25(16):2078–2079.

644 [73] Gaspar JM. Improved peak-calling with MACS2. *BioRxiv*. 2018; p. 496521.

645 [74] Li Q, Brown JB, Huang H, Bickel PJ. Measuring reproducibility of high-throughput experiments. *The
646 annals of applied statistics*. 2011;5(3):1752–1779.

647 [75] Newell R, Pienaar R, Balderson B, Piper M, Essebier A, Bodén M. ChIP-R: Assembling reproducible
648 sets of ChIP-seq and ATAC-seq peaks from multiple replicates. *Genomics*. 2021;113(4):1855–1866.

649 [76] Virtanen P, Gommers R, Oliphant TE, Haberland M, Reddy T, Cournapeau D, et al. SciPy 1.0:
650 Fundamental Algorithms for Scientific Computing in Python. *Nature Methods*. 2020;17:261–272.
651 doi:10.1038/s41592-019-0686-2.

652 [77] Efron B. Nonparametric estimates of standard error: the jackknife, the bootstrap and other methods.
653 *Biometrika*. 1981;68(3):589–599.

654 [78] John Lu Z. *The elements of statistical learning: data mining, inference, and prediction*; 2010.